INTERNATIONAL ATOMIC ENERGY AGENCY
UNITED NATIONS EDUCATIONAL, SCIENTIFIC AND CULTURAL ORGANIZATION
INTERNATIONAL CENTRE FOR THEORETICAL PHYSICS
I.C.T.P., P.O. BOX 586, 34100 TRIESTE, ITALY. CABLE CENTRATOM TRIESTE

SMR.703 - 19

WORKING PARTY ON
MECHANICAL PROPERTIES OF INTERFACES

23 AUGUST - 3 SEPTEMBER 1993

"High Temperature Failure in Ceramics" (Part I)

"Influence of Microstructure on Creep Rupture" and "Creep and Creep Rupture of Structural Ceramics"

Sheldon WIEDERHORN
United States Department of Commerce
National Institute of Standards and Technology
Materials Science and Engineering Laboratory
Building 233, Room B309
Gaithersburg, MD 20899
U.S.A.

STRADA COSTIERA 11 - TELEPHONE 224531 - TELEX 460392

From: CERAMIC MICROSTRUCTURES '86
Edited by Pask and Evans
(Plenum Publishing Corporation, 1988)

INFLUENCE OF MICROSTRUCTURE ON CREEP RUPTURE

S.M. Wiederhorn, B.J. Hockey and R.F. Krause, Jr.

National Bureau of Standards
Institute for Materials Science and Engineering
Gaithersburg, MD 20899

ABSTRACT

In this paper, the effect of microstructure on both the creep and creep rupture behavior of two commercial grades of vitreous bonded aluminum oxide was investigated. Deformation and fracture occurred within the ductile, intergranular phase of the material. The creep rate was relatively insensitive to the amount of intergranular phase, but was sensitive to structural details of that phase. The creep rate could be reduced by increasing both the degree of crystallization of the intergranular phase and the viscosity of residual glass within that phase. The time-to-rupture and the strain-at-rupture increased as the amount of intergranular phase within the material increased. In this regard, an increase in the amount of intergranular phase permitted greater accommodation of strain, and hence, blunting of cavities that nucleated during the creep process. The data fit a modified Monkman-Grant curve in which the Monkman-Grant coefficient was sensitive to both stress and the amount of intergranular phase. The Monkman-Grant coefficient was not sensitive, however, to the degree of crystallization of the intergranular phase.

INTRODUCTION

A common method of manufacturing ceramics involves the use of chemical aids that permit sintering at reduced temperatures. Sintering aids are, in fact, essential in the manufacture of many covalent materials such as silicon nitride and silicon carbide, since these materials do not sinter easily without them. With the addition of sintering aids, sintering occurs by liquid phase transport, which enhances the densification rate. As the temperature is reduced, the sintering aid solidifies and a dense, rigid solid forms. However, a residual low melting phase is invariably left at the grain boundaries so that when the temperature is raised again the phase softens, thereby establishing a thermal limit for use of the material in high temperature applications. Quantification of the effect of second phases on creep and creep rupture is relevant, therefore, to establishing upper temperature bounds for the use of ceramic materials in high temperature applications

Since intergranular phases in ceramics made with sintering aids are often vitreous at high temperatures, an understanding of the effect of

phase composition, devitrification at lower temperatures and the amount of the second phase on creep and creep rupture is important for improving ceramic performance in high temperature structural applications. With this in mind, the effect of intergranular phases on the mechanical behavior of ceramic materials at high temperatures was studied using two, microstructurally different alumina ceramics as model materials. Both the amount of intergranular phase and the degree of crystallization were used as experimental variables.

EXPERIMENTAL PROCEDURE

Two commercial grades of vitreous bonded aluminum oxide were selected for study primarily because they contained significantly different volume fractions of intergranular phase. One (COORS AD-96) contained approximately 6 to 8 vol. % intergranular silicate phase, the other (COORS AD-85) contained approximately 20 to 25 vol. % intergranular silicate phase. All mechanical tests were conducted in four-point bending using a fixture with an outer gauge section of 40 mm and an inner gauge section of 10 mm. Specimens, 50 by 5 by 3 mm, were obtained from large blocks of material by diamond sawing and grinding. After the final grinding step, specimens were annealed at 1050°C for 96 hr. to stabilize the microstructure prior to the creep studies. Tests were conducted in the temperature range 950°C to 1100°C for AD-96 and 1000°C to 1150°C for AD-85.

Creep studies were conducted by the method described earlier [1]. Creep rates were determined from the load point displacement using the method of Hollenberg et al. [2], assuming linear flow in the material. No corrections were made for non linear creep or for possible shifts in the neutral axis as a consequence of unequal creep in compression and tension [3-5]. Investigations of the microstructure of these materials were conducted primarily by analytical transmission electron microscopy. The composition of the intergranular glass in as-received, annealed, and deformed material were determined by x-ray energy dispersive spectroscopy, while crystalline devitrification products were identified by both x-ray diffraction analysis and x-ray energy dispersive spectroscopy. Microstructural analyses were conducted on both the compressive and tensile sections of test specimens.

EXPERIMENTAL RESULTS

Microstructure

Figure 1 compares polished sections of AD-85 and AD-96 to illustrate some of the important differences in the structure of the two aluminas used in this study. While both aluminas are primarily composed of Al_2O_3 grains of varying size and shape, there is a clear difference in average grain size. On the basis of the line intercept method, an average grain size of ~ 9 μm is obtained for AD-96 and ~ 3 μm for the AD-85. On the same basis, the volume fraction of intergranular, binding phase ranged from ~0.2 to ~0.25 in the AD-85 and from ~0.06 to ~0.08 in AD-96. Both aluminas also contained an undetermined volume fraction of porosity, typically in the form of isolated grain-size pores, Figure 1, which from post-test examinations did not appear to play a significant role in the deformation or rupture processes.

Closer examination of the microstructure of both materials by transmission electron microscopy, Figures 2-4, revealed the presence of a binder phase not only at multi-grain junctions (as indicated in Figure 1), but also between all adjacent Al_2O_3 grains. Thus, while it is convenient to distinguish between multi-grain junction regions and grain

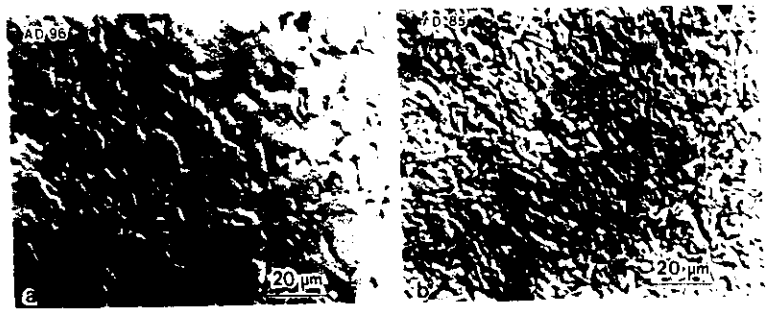

Fig. 1. Optical micrographs of relief-polished (a) AD-96 and (b) AD-85 illustrating differences in grain size and volume fraction of intergranular phase for the two aluminas.

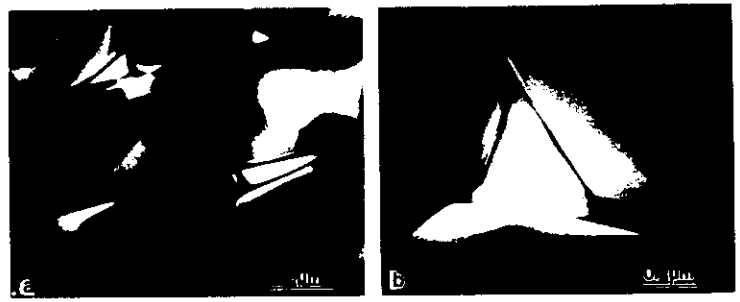

Fig. 2. Transmission electron micrographs illustrating the microstructure of vitreous bonded AD-96 alumina in the as-received state. Glass of uniform composition is located at triple junctions (a and b) and also between adjacent grains (b).

boundary layers, the intergranular space is continuous. Consistent with the inhomogeneous Al_2O_3 grain morphology, there was a considerable variation in the dimensions of individual multi-grain junction regions and in the widths of intergranular layers found in both aluminas. Typically, the former ranged in size and shape from micron-sized, irregular shaped "pockets" to smaller (tenths of a micron), triangular shaped triple junctions, Fig. 2a; intergranular layer widths ranged from tenths of a micron down to an apparent limiting width of nanometer dimensions, Fig. 2b. Due to the differences in grain size and in volume fraction of binder phase for the two aluminas the intergranular widths in AD-96 were, on the average, narrower as well as longer than those in the AD-85. In addition to these dimensional differences, the intergranular phase in AD-96 was found to be entirely glassy in the as-received condition, whereas in AD-85 the intergranular regions contained either glass or crystalline anorthite, Figure 3. Table 1 lists the initial intergranular glass phase compositions for both AD-96 and AD-85. Also included in Table 1 are data obtained on an AD-85 sample in which the intergranular phase was made entirely glassy by quenching from 1400°C.

Although comparison of the "as-received" glass compositions indicates

TABLE I: GLASS PHASE COMPOSITIONS (wt. %)

	SiO_2	Al_2O_3	MgO	CaO	FeO	Na_2O	K_2O	BaO
AD96*	54.7	25.3	8.3	2.7	0.9	7.3	0.8	-
AD85*	57.8	21.1	5.5	3.3	1.3	-	-	11.0
AD85**	50.1	29.5	5.1	8.2	0.6	-	-	6.5

*As-Received
**Quenched from 1400°C

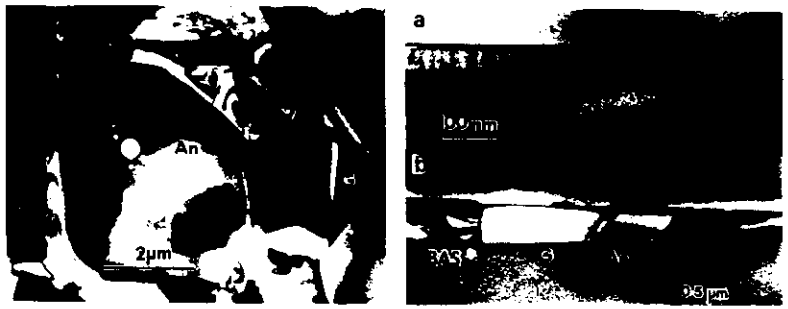

Fig. 3. (left) Transmission electron micrograph from AD-85 alumina in the as-received condition. Intergranular phase is largely contained within multi-grains junctions and consists of glass and crystalline (anorthite) phases.

Fig. 4. (right) Transmission electron micrographs illustrating the glassy to crystalline phase change that occurs within grain boundaries during creep. In AD-96 (a), devitrification resulted in the exclusive formation of plagioclase (~0.5 albite/0.5 anorthite). In AD-85, most grain boundaries similarly crystallized to anorthite or contained multiple phases of anorthite (An), celsian (BAS), and/or cordierite separated by a high silica glass (G), as in (b).

a significant difference only with regard to the presence and concentrations of Na_2O and BaO, considerable differences were found in both the nature and distribution of crystalline, intergranular phases produced when the two aluminas were exposed to high temperatures, either during static annealing treatments or during the creep tests. As described in an earlier paper on the flexural creep of AD-96 [1], the extent of devitrification, the nature and distribution of intergranular phases, and the composition of retained glass in this alumina all depend not only on proximity to external surfaces, but on the state of stress. Specifically it was shown that considerably greater crystallization of the initially glassy binder phase occurs within the tensile zone as compared to the neutral or compressive zones, and that this can be directly related to the additional crystallization of a plagioclase phase. Moreover, plagioclase was found to form not only within multi-grain junctions, but also within many of the narrower (≤ 200 nm) grain boundary regions, Figure 4a, whereas the various other crystalline products of devitrification (i.e. the magnesio-alumino-silicates, enstatite, sapphirine, and corderite) formed only within multi-grain junctions. Thus during creep, grain boundaries within the tensile regions of AD-96 consist primarily of crystalline plagioclase and/or

retained glass, while those within the compressive zone (excluding the near surface regions) are entirely glassy.

As indicated above, the as-received state of AD-85 differs from the AD-96 in that a significant fraction of the intergranular regions (including both grain boundary layers and multi-grain junctions) is crystalline anorthite. While the bulk distribution of intergranular phases developed in flexural creep samples was not investigated, examination of thin sections taken parallel to and immediately beneath the exposed tensile and compressive surfaces revealed extensive devitrification due to the formation of additional anorthite together with corderite, sapphirine, and a barium aluminosilicate, tentatively identified as silica-rich celesian. While anorthite appeared to be the primary crystalline phase present within the narrower grain boundaries (i.e. 200 nm or less in width), many grain boundaries were also found to be composed of corderite (usually with an inter-dispersed glass phase), or combinations of all four crystalline phases separated by glass, Figure 4b. The composition of retained glass found in devitrified AD-85 also differed somewhat from that found in devitrified AD-96. In AD-96, devitrification resulted in a retained glass phase significantly depleted in all of the network modifiers, but still containing roughly 20 % by weight Al_2O_3, whereas in AD-85 the retained glass phase was significantly depleted in Al_2O_3 as well and often appeared to be pure SiO_2.

Creep Measurement

The effect of devitrification on the creep rate of AD-96 is illustrated in Figure 5. The creep rate of the fully vitreous (as-received) material is approximately one hundred times that of the devitrified (annealed) material. Furthermore, failure occurs in only ~25 minutes for the vitreous material compared to ~60 hours in the devitrified material under identical test conditions. The estimated increase in viscosity of the retained glass in the annealed material can only account for a decrease in the creep rate by a factor of 10 [1]. The additional factor of 10 decrease in the observed creep rate must be due to the presence of intergranular crystalline phases, which are undoubtedly more resistant to flow than glass of a similar composition [1]. Although a comparison of vitreous AD-85 with fully devitrified AD-85 has not been made, a similar reduction of creep rate by devitrification is also expected for this material.

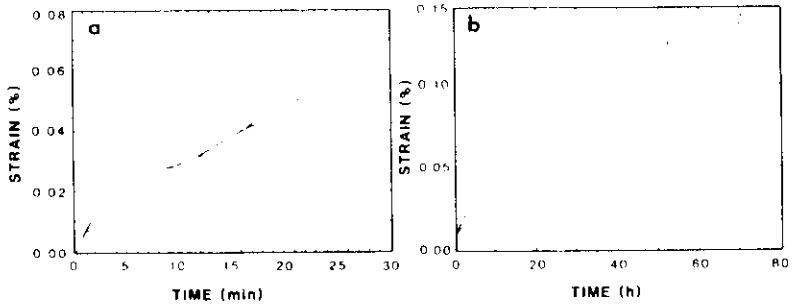

Fig. 5. The effect of devitrification on the creep rate of AD-96: (a) As-received material; (b) Material that has been annealed at 1050°C for 96 hours. The creep rate of the as-received material is approximately one hundred times that of the fully devitrified material. Solid and dashed lines represent independent runs.

Creep of the AD-96 specimens usually ended in failure at a strain of from ~0.05 to ~0.15 percent [6]. By contrast, very few of the AD-85 specimens failed within the times of the experiments, which in certain cases exceeded 700 hrs. Those AD-85 specimens that did fail, failed at a strain that ranged from ~0.4 to ~1.4 percent. Thus, the strain required for failure of the AD-85 was approximately ten times that of the AD-96. Despite this difference in rupture strain, both materials appeared to exhibit primary creep over most of the test range. For both types of materials, the creep strain, ϵ, could be expressed in terms of a power function in time, with a fractional time exponent, n: $\epsilon = \epsilon_0 t^n$. For all studies, the value of n ranged from 0.4 to 0.6.

The creep behavior of the AD-85 and the AD-96 are compared in Figure 6 for two test conditions: one in which failure of the AD-96 sample occurred within a few hours of initial load; the other in which the time to failure was approximately 100 hours. Under the same test conditions, the AD-85 samples sustained the load for the entire duration of the tests, which were eventually interrupted before failure. Aside from the difference in the time-to-rupture, the most significant result of the study was the relative insensitivity of the creep rate to the material being tested. For the shorter of the two runs, Figure 6a, the creep rate was essentially identical for both materials over the entire test range. For the longer of the two runs, Figure 6b, the creep was faster for the AD-85, but only by a factor of two or three at a given strain. Thus, the creep rate of AD-96 just prior to failure was 1.89×10^{-9} s^{-1}, whereas the creep rate of the AD-85 at the same strain was 4.69×10^{-9} s^{-1}.

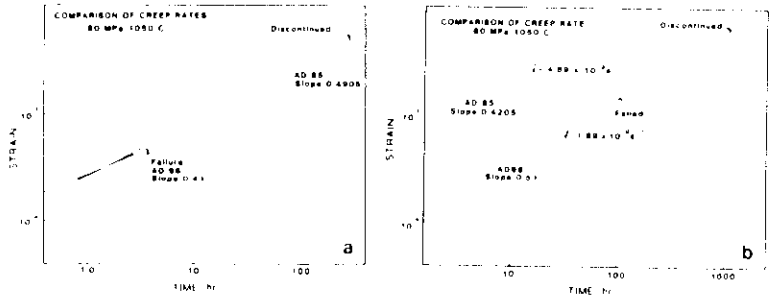

Fig. 6 The creep behavior of AD 85 and AD 96 compared for two test conditions: (a) failure of the AD-96 occurred within a few hours of initial load; (b) failure of the AD-96 occurred in approximately 100 hours.

Cavitation and Crack Morphology

In both aluminas crack initiation and incremental growth occur by a selective cavitation process in which cavitation first occurs within relatively narrow grain boundaries that are roughly aligned normal to the tensile axis. Subsequently, cavitation occurs within inclined grain boundaries and multi-grain junctions to form a continuously open crack. Examination of isolated, partially cavitated grain boundaries by transmission electron microscopy, moreover, has shown that cavities appear to nucleate preferentially within the glassy portions of grain boundaries, since cavities are invariably bounded by a residual glass phase. Figure 7 illustrates the almost identical manner in which cavitation first occurs within relatively narrow grain boundary layers in both materials. In both examples seen in Figure 7, the grain boundary

phase was glassy throughout, whereas in Figure 8 cavitation in AD-85 occurred within a wider, partially crystallized grain boundary, and a glassy phase of nearly pure SiO_2 separates the cavity from the crystalline anorthite phase. While the initial stages of crack development in both materials can be similarly described by this selective cavitation process, the eventual morphology of the cracks is quite different and this difference can be related to differences in grain size and volume fraction of binder phase.

Fig. 7. (left) Transmission electron micrographs showing cavities formed within narrow grain boundaries in (a) AD-96 and (b) AD-85. In both aluminas, grain boundary cavitation represents the initial stage in creep crack formation.

Fig. 8 (right) Transmission electron micrograph of partially cavitated grain boundary region in AD 85. Note presence of nearly pure silica glass (G) between expanding cavity (C) and intergranular anorthite (An)

In AD-96 selective cavitation of grain boundaries oriented normal to the tensile axis results in "segmented cracks" consisting of cavitated and partially cavitated grain boundaries, Figure 9a. These cracks grow stably to macroscopic dimensions while retaining relatively narrow opening displacements due to the restraining actions of the partially cavitated grain boundary segments. Further deformation eventually results in the development of stresses sufficient to separate the restraining grain boundary segments, and ultimately catastrophic failure occurs. In this process relatively little cavitation occurs along the flanks of cracks in AD-96; instead, cavitation is mainly restricted to favorably oriented grain boundaries ahead of the advancing crack. In many ways the manner in which creep cracks in AD-96 grow closely resembles the description of crack growth in recently developed crack interface bridging models, which have been proposed to explain the effect of microstructure on fracture toughness [7].

In AD-85, the initial stage of crack development and crack growth also involves the selective cavitation of narrow, favorably oriented grain boundaries. However, because of the smaller grain size and larger volume fraction of intergranular phase for this material (relative to AD-96), the cavitated grain boundaries are not only smaller and more uniformly distributed but tend to be separated from each other by micron-sized multi-grain junctions. As a consequence, continued cavity growth, leading to the formation and growth of cracks of multiple grain size dimensions, is effectively arrested until the development of higher local strains sufficient to drive the cavitation process through the interleaving multi-grain junctions. Thus, unlike the "segmented cracks" that form in AD-96, Figure 9a creep cracks in AD-85 necessarily attain a

fully open morphology and, with continued growth, exhibit appreciable crack opening displacements, Figure 9b. Moreover, because of the enhanced capacity of AD-85 to distribute and accommodate strain - as evidenced by the large crack openi..g displacements - individual crack segments generally arrest within 200 to 300 μm. Nevertheless, continuous cracks of macroscopic dimensions, eventually responsible for failure in AD-85, develop by the linking up of similar, adjacent crack segments.

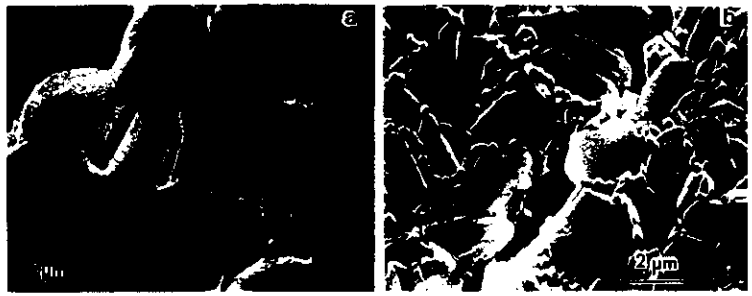

Fig. 9. Scanning electron micrographs illustrating representative portions of creep cracks developed at tensile surfaces in (a) AD-96 and (b) AD-85. Distinct differences in crack morphology and crack opening displacements relate to the effect of microstructure on crack growth by cavitation, as discussed in the text.

DISCUSSION

Two Phase Creep

A number of theories have been developed to explain the creep of two phase materials. All assume homogeneous deformation of the structure, so that each grain of the structure contributes a proportional amount to the total deformation. Creep models can be divided into three types: lubricated flow [8, 9]; percolation [9, 10]; and, solution-precipitation [8, 11-16]. In lubricated flow, the second phase acts as a lubricant reducing the friction between adjacent solid particles during shear deformation. In percolation, localized flow of fluid from the compressive to the tensile surfaces of individual grains governs deformation. Finally, in solution-precipitation, mass transport of the solid grains through the liquid controls the deformation rate. Each of these theories suggests that the steady state creep rate is inversely proportional to the viscosity of the second phase fluid, a result that is consistent with our finding that the creep rate is reduced when the effective viscosity of the intergranular phase is increased by devitrification.

Current theories of creep also suggest a dependence of the creep rate on microstructure: in particular on the grain size, g, of the material and on the fraction of second phase, w/g, present in the material (w is the thickness of the intergranular phase). In lubricated flow, the creep rate is expected to be proportional to w/g, in percolation to $(w/g)^3$, and in solution-precipitation to w/g if the process is interface controlled [12] and to $(w/g)/g^2$ if the process is transport controlled [12]. For the materials studied in the present paper, the measured 3:1 ratio (AD-96 to AD-85) of grain size and volume fraction of second phase (AD-85 to AD-96) should result in an increase of creep rate (AD-85 relative to AD-96) of ~30 for the percolation or transport controlled solution-precipitation and ~3 for simple sliding or interface controlled solution-precipitation, provided the effective viscosity of the second phase in both materials is the same. From the present results one must conclude that neither transport controlled solution-precipitation, nor percolation can account for the observed results. Simple lubrication also does not provide an adequate explanation of the results because it does not account for the dilatation that occurs during the creep of two phase materials [17, 18]. Furthermore, simple lubrication does not provide sufficient resistance to flow to account for the low creep rates measured in the present study [8, 9]. Therefore, interface controlled solution precipitation [12] appears to be the most likely mechanism to explain the present set of data[1].

Creep-Rupture

Creep rupture data on structural materials is often summarized in terms of a Monkman-Grant [20] plot, in which the minimum strain rate, $\dot{\epsilon}_{min}$, is plotted as a function of the stress rupture time, t_r. Originally devised to correlate data on structural metals, the plot provides a simple way of summarizing creep data since the creep rate is often found to be inversely proportional to the failure time. In the present study the grain boundary phase was modified in two ways in order to influence the creep and creep rupture behavior: (1) annealing was used to devitrify the material in hopes of increasing the time to failure; (2) a material with additional second phase was tested with the expectation of increasing the strain to failure. Both treatments enhanced the creep rupture lifetime. For practical purposes it is important to ascertain whether these microstructural modifications can also change creep-rupture behavior when this behavior is expressed in terms of the Monkman-Grant relation.

A comparison of the creep rupture behavior of the as-received (fully vitreous) and annealed (devitrified) AD-96 is shown in figure 10a. In earlier studies of this material, annealed specimens were shown to obey a modified Monkman-Grant relation in which the Monkman-Grant constant was a function of stress [1]. The data seemed to indicate that for a fixed value of the applied stress, a linear relation is obtained between the creep rate and the inverse of the rupture time. Included with the results of the earlier study are the creep rupture results from the as-received AD-96, which was tested at 60 MPa (Figure 5). The rupture data for the as-received material fall on the same line as the other AD-96 data collected at the same applied stress. This result suggests that Monkman-Grant curves for this material are not affected by the state of crystallization of the second phase as long as the grain size and the relative amount of the second phase are constant. For this condition, the rupture time can be predicted in terms of the creep rate regardless of the state of devitrification.

By contrast, changing the volume of the second phase seems to have a significant effect on the position of the Monkman-Grant curve. This result is illustrated in Figure 10b, in which data from the specimens of AD-85 that failed are plotted with data from specimens of AD-96. Because of the limited amount of data for AD-85, the data are compared at constant temperature rather than at constant stress. All of the data for the AD-96 fall on straight lines of constant temperature (for this type

[1]Wang and Raj [18] in their investigation of the creep of glass-ceramics found that the mechanism of creep that was most consistent with their data was transport controlled solution-precipitation.

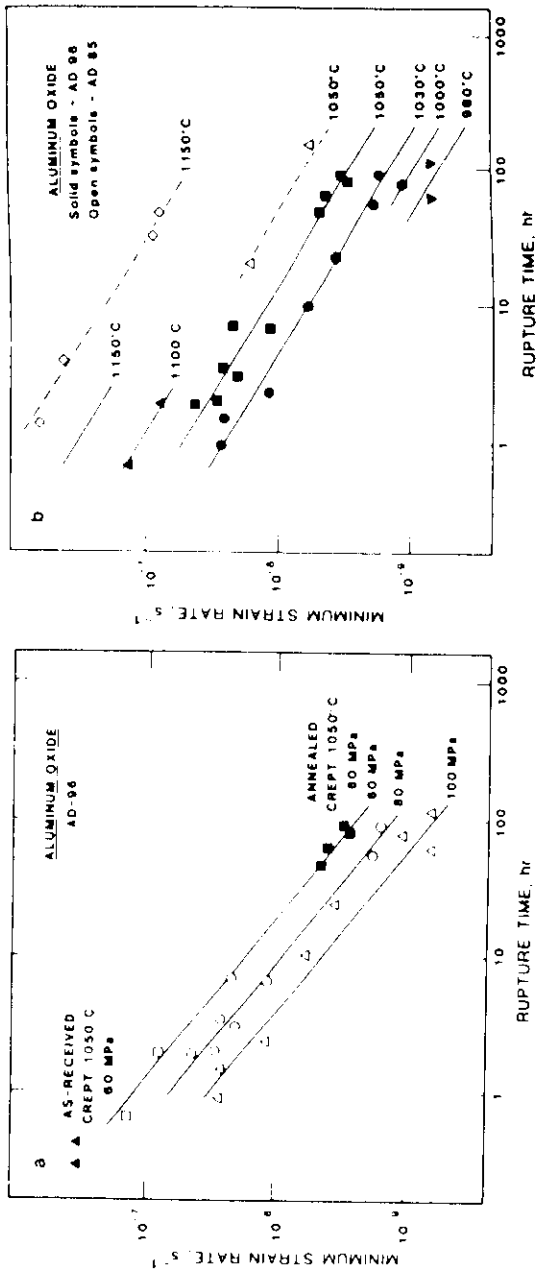

Fig. 10. Creep rupture data expressed in terms of Monkman-Grant curves. In (a), the creep rupture behavior of the as-received and fully devitrified AD-96 is compared. Note that for the same test conditions, the data for the glass bonded material, solid triangles, falls on the same line as the data for the devitrified material, solid squares. In (b), data for the AD-96 are compared with those for the AD-85. Because of the limited amount of data on the AD-85, the data are compared at constant temperature rather than at constant stress.

of representation, the slopes of the lines are not -1). The data for the AD-85 fall on a set of lines that are displaced from the lines for the AD-96 by a factor of approximately 3 in time at a constant creep rate. As the creep rate for a given strain is not sensitive to the amount of second phase, figure 6, it must be concluded that the difference in behavior of the two materials is primarily a consequence of the greater tolerance of the AD-85 to strain. The greater capacity for accommodation in the AD-85 yields a material with a very different stress rupture behavior.

ACKNOWLEDGEMENT

Support of the Department of Energy, Automotive Gas Turbine Program is gratefully acknowledged.

REFERENCES

1. S.M. Wiederhorn, B.J. Hockey, R.F. Krause, Jr. and K. Jakus, "Creep and Fracture of a Vitreous-Bonded Aluminum Oxide," J. Mater. Sci. 21, 810-824 (1986).

2. C.W. Hollenberg, G.R. Terwilliger and R.S. Gordon, "Calculation of Stress and Strains in Four-Point Bending Creep Tests," J. Am. Ceram Soc. 54, 196-199 (1971).

3. S.M. Wiederhorn, L. Chuck, E.R. Fuller, Jr. and N.J. Tighe, "Creep Rupture of Siliconized Silicon Carbide," pp. 755-774 in Tailoring Multiphase Ceramics, R.E. Tressler, G.L. Messing and C.G. Pantano, eds., Plenum Press, New York (1987).

4. D.F. Carroll, R.E. Tressler, Y. Tsai and C. Near, "High Temperature Mechanical Properties of Siliconized Silicon Carbide Composites," pp. 775-788 in ref. 3.

5. H. Cohrt, G. Grathwohl and F. Thummler, "Strengthening after Creep of Reaction-Bonded Siliconized Silicon Carbide," pp. 515-526 in Creep and Fracture of Engineering Materials and Structures, B. Wilshire and D.R.J. Owen, eds., Pineridge Press, Swansea, U.K. (1984).

6. K. Jakus, S.M. Wiederhorn and B.J. Hockey, "Nucleation and Growth of Cracks in Vitreous-Bonded Aluminum Oxide at Elevated Temperatures," J. Am. Ceram. Soc. 69 (1986) October issue.

7. P.L. Swanson, C.J. Fairbanks, B.R. Lawn, Y-W Mai and B.J. Hockey, "Crack-Interface Grain Bridging as a Fracture Resistance Mechanism in Ceramics: I. Experimental Study on Alumina," J. Am. Ceram. Soc., in press (1987).

8. G.M. Pharr and M.F. Ashby, "On Creep Enhanced by a Liquid Phase," Acta Met. 31, 129-38 (1983).

9. F.F. Lange, "Non-Elastic Deformation of Polycrystals with a Liquid Boundary Phase," pp. 361-381 in Deformation of Ceramic Materials, R.C. Bradt and R.E. Tressler, eds. Plenum Press, New York (1975).

10. D.C. Drucker, "Engineering and Continuum Aspects of High-Strength Materials," pp. 795-833 in High Strength Materials, V.F. Zackay, ed., John Wiley and Sons, Inc., New York (1965).

11. R. Raj, "Creep in Polycrystalline Aggregates by Matter Transport Through a Liquid Phase," J. Geophys. Res. 87 [B6], 4731-39 (1982).

12. R. Raj and C.K. Chyung, "Solution-Precipitation Creep in Glass Ceramics," Acta Met. 29, 159-66 (1981).

13. D.W. Durney, "Solution-transfer, an Important Geological Deformation Mechanism," Nature, 235, 315-16 (1972).

14. D.W. Durney, "Pressure Solution and Crystallization Deformation," Phil. Trans. R. Soc. A283, 229-40 (1976).

15. E.H. Rutter, "The Kinetics of Rock Deformation by Pressure Solution," Phil. Trans. R. Soc. Lond. A283, 203-219 (1976).

16. R.L. Stocker and M.F. Ashby, "On the Rheology of the Upper Mantle," Rev. Geophys. and Space Phys. 11, 391-421 (1973).

17. O. Reynolds, "On the Dilatancy of Media Composed of Rigid Particles in Contact, with Experimental Illustrations," Phil. Mag. 20, 469-81 (1885).

18. F.C. Frank, "On Dilatancy in Relation to Seismic Sources," Rev. Geophysics, 3, 485 (1965).

19. J.-G. Wang and R. Raj, "Mechanisms of Superplastic Flow in a Fine-Grained Ceramic Containing some Liquid Phase," J. Am. Ceram. Soc. 67, 399-409 (1984).

20. F.C. Monkman and N.J. Grant, "An Empirical Relationship between Rupture Life and Minimum Creep Rate in Creep-Rupture Tests," Proc. ASTM 56, 593-620 (1956).

CREEP AND CREEP RUPTURE OF STRUCTURAL CERAMICS

S.M. WIEDERHORN, B.J. HOCKEY and T.-J. CHUANG
National Institute of Standards and Technology
Gaithersburg, MD 20899, USA

ABSTRACT. Structural ceramics are often two phase materials, in which rigid refractory grains, fibers, or whiskers are bonded by a less refractory matrix. At elevated temperatures, creep occurs by deformation of the matrix, resulting in the localization of stresses along grain boundaries, followed by cavitation and eventually by structural failure of the ceramic. The sequence of events prior to failure depends on the grain size and the amount of bonding matrix within the solid. Large amounts of matrix phase reduce constraints at grain boundaries, and thus the stresses that cause cavitation. Large grains, fibers or whiskers provide easy paths for crack growth, so that, once initiated, cracks readily propagate to failure. In structural ceramics, failure time can be expressed as a power function of the creep rate; the coefficient and exponent of the power function are determined by the failure mechanism. In this paper, models for creep rupture of ceramics are presented for cavity coalescence and for crack growth as primary failure processes. The model for cavity coalescence, in particular, is used to rationalize creep rupture data for a two phase ceramic that fails by cavity coalescence.

1. INTRODUCTION

Failure of structural ceramics at elevated temperatures can be classified into two general types depending on the time required for failure [1-5]. For relatively short failure times, failure is a consequence of crack growth from preexisting defects. For relatively long failure times, failure results from distributed cavities that are nucleated by the creep process. A threshold stress separates the two types of failure [2]. Most theoretical and experimental work on ceramics at elevated temperatures have dealt with crack growth as the principal mode of failure and a series of excellent reviews and research papers are available on this subject [6-8]. The subjects of cavity nucleation and cavity growth in ceramic materials have also been investigated and are similarly referenced in the literature [9-12]. With few exceptions [13], an area of the ceramics literature that has been neglected is cavity coalescence, which pertains to the sequence of events that transforms cavities into microcracks.

Cavity coalescence is the main subject of this paper. First, the steps leading to the formation of cavities and/or microcracks are discussed and are shown to be critically dependent on the microstructure of the ceramic. Whether microcracks, or isolated cavities are formed during cavitation is shown to depend on the ratio of the volume of bonding matrix to the volume of the refractory grains, and also on the size and shape of the refractory grains in the

S. P. Shah (ed.), Toughening Mechanisms in Quasi-Brittle Materials, 555-576

structural ceramic. Next, it is shown that the creep life of two phase ceramics can be expressed as a power function of the strain rate, independent of temperature or applied stress. This relation between creep rate and failure time was first proposed by Monkman and Grant [14] for structural alloys. It also provides a convenient representation for analyzing creep rupture data in structural ceramics. Finally, two theories to rationalize the dependence of rupture life on creep rate are developed. Of these, a theory modelled on cavity coalescence is shown to provide a satisfactory description of the stress rupture behavior of a ceramic that forms isolated cavities during deformation.

2. CAVITY MORPHOLOGY

All materials discussed in this paper are two phase ceramics, in which refractory grains or whiskers are surrounded and bonded by a less refractory matrix. The grains are assumed to be completely rigid so that all deformation occurs within the matrix. This assumption is valid for a wide class of structural ceramics over a range of conditions[1]. Despite differences in the microstructures of these two phase materials, certain common features are apparent both in the mode of cavitation, and in the way cavities grow in these materials. First, cavities always seemed to form at interfaces between the rigid grains and the more ductile matrix. Most often, cavities are observed to form within the interfacial regions separating closely spaced grains, or at triple junctions. Interfacial cavitation is illustrated in figure 1 for two grades of alumina [16], and in figure 2 for a grade of siliconized silicon carbide [17-18]. Cavities form at such locations largely because of physical limitations on the rate of flow of the matrix between the grains as they move apart [19, 20]. If the matrix does not flow rapidly enough, high dilational stresses develop within the matrix, eventually resulting in the formation of cavities. Since the highest stresses develop at the midpoint between two planes that are being pulled apart, cavitation is expected to occur preferentially between grains that are closely spaced.

A quantitative estimate of the stresses that develop between two grain interfaces can be obtained by modeling the interfaces by two circular cylinders of radius G, separated by a distance h, figure 3. As the cylinders are forced to move apart, fluid is sucked into the space between the cylinders. Assuming no slip between the fluid and the disk, the pressure, p, that develops between the cylinders is given by the following relation [21]:

$$p = p_o - (3 \cdot \mu / h^3) \cdot (dh/dt) \cdot (G^2 - g^2) \qquad (1)$$

[1] As the refractoriness of the matrix phase increases relative to that of the grains, higher temperatures have to be used to deform the solid. As a consequence, deformation and hence cavitation may also occur within the grains, at the grain boundaries. Such cavitation has been observed in one of the newer grades of silicon nitride, in which small lenticular shaped cavities decorate the grain boundaries of the solid after creep at elevated temperatures [15]. The morphologies of these cavities is essentially different from those discussed below.

Figure 1. Transmission electron micrographs showing cavities formed within narrow grain boundaries in (a) AD-96 and (b) AD-85. In both grades of alumina, grain boundary cavitation represents the initial stage in creep crack formation. Microstructural analysis indicates grain sizes of ≈9μm and ≈3μm for AD 96 and AD-85, respectively. AD-96 contains 96 wght. % aluminum oxide, whereas AD 85 contains 85 wght. % aluminum oxide. The volume fraction of intergranular binding phase ranged from ≈0.2 to ≈0.25 for the AD-85 and from ≈0.06 to ≈0.08 for the AD-96. Data from reference 16.

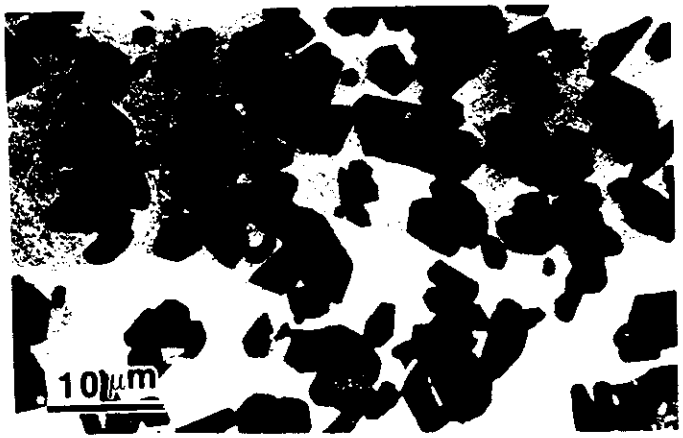

Figure 2. Cavity formation in Carborundum KX01. This material contains ≈33 vol. % silicon. Cavities are always located at Si/SiC interfaces, most often between two closely spaced SiC grains. As the cavities grow from the narrow space between the grains, they arrest on encountering a larger pool of silicon. The applied tensile stress was vertical (top to bottom) in the figure.

where g is the distance from the center of the cylinder, p_o is the pressure in the fluid surrounding the cylinders and μ is the viscosity of the fluid. The maximum absolute pressure occurs when g = 0. If the grains in a material are considered to be rigid cylinders of height 2G, then $dh/dt \approx 2G \cdot \dot{\varepsilon}$, so that

$$p - p_o = 6 \cdot \dot{\varepsilon} \cdot \mu \cdot (G/h)^3 \qquad (2)$$

For the grade of siliconized silicon carbide shown in figure 2, a viscosity of 10^{13} Pa·s is estimated at 1300°C and 100 MPa from the creep map for silicon[22]. For a creep rate of $\approx 10^{-8}$ s^{-1}, and a SiC grain size of 5μm, pressures >1 GPa are estimated for values of h <2Inm. Grain boundary separations of this magnitude are not unusual for SiC bonded by Si, suggesting that cavitation should be relatively easy once the creep rate has exceeded a threshold value determined by the grain separation.

Once nucleated, a cavity tends to grow along the grain interface until it covers the facet of the grain on which it nucleated. Subsequent growth then depends on the microstructure of the solid. If only a small amount of bonding phase is at the grain interface, the cavity will continue to grow from one grain to the next along grain interfaces, thus forming a crack. Such crack formation

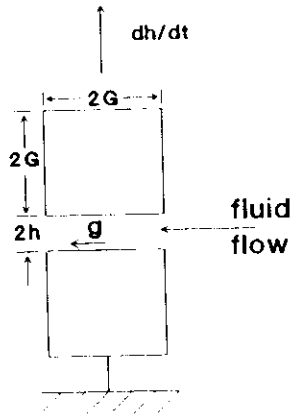

Figure 3. Model of two grains being pulled apart as a consequence of the creep process. Fluid is assumed to flow freely into the space between the two grains, establishing a pressure gradient, which is the cause of cavitation. The bonding matrix is assumed to be approximated by a viscous fluid in this model.

[2] In this estimate a grain size of 5 μm is assumed for the silicon carbide grains. The viscosity of silicon is calculated as the ratio of the applied stress to the creep rate at 1300°C. As silicon is a power-law material, it is recognized that equation 2 can only approximate the true situation.

via rapid interfacial cavity growth was typically observed in alumina containing ≈8 vol. % glass, figure 4. Similar creep crack formation due to small amounts of glass at grain boundaries has also been observed by Evans et al. [23] and by Wilkinson [24] in studies on nominally "pure" alumina containing isolated pockets of glass. In these materials, the glass wets the grain boundaries of the aluminum oxide grains only in the vicinity of the glass pockets. Under stress, cracks readily generated from the glass pockets, then grew into the bulk of the alumina where they arrested. Thus, in small quantities, glass apparently "embrittles" aluminum oxide at elevated temperatures, permitting the nucleation of sizable cracks within the material as a consequence of creep cavitation.

As the volume fraction of bonding phase within the solid is increased, cavities tend to stabilize once they have propagated across a facet. This is illustrated for a grade of siliconized silicon carbide containing 33 vol. % silicon (Carborundum KX01), in which isolated damage occurs as a consequence of cavitation, figure 2. After a nucleus is formed between two narrowly spaced grains, cavities generally grow until they intersect the larger pockets of silicon on each side of the boundary. The cavity then blunts and arrests. Cavities are formed at random throughout the gauge section and, with continued creep, the gauge section becomes filled with these cavities. For this type of cavitation, cavity coalescence is required to form a crack that then propagates through the material causing failure, figure 5.

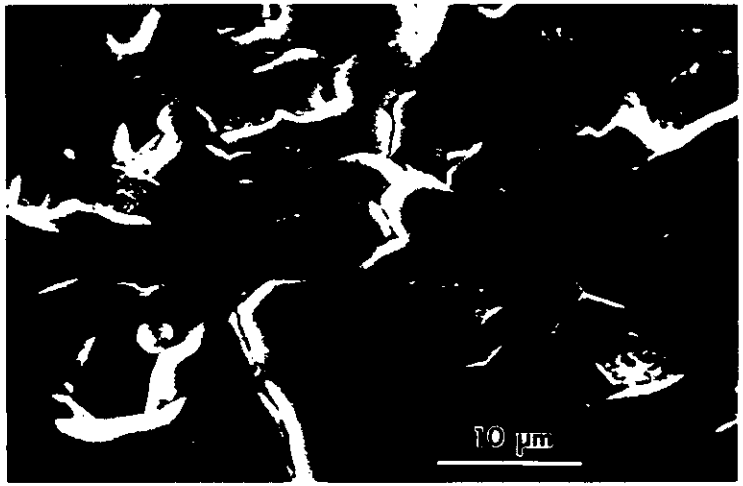

Figure 4. Scanning electron micrograph illustrating representative portion of a creep crack developed at the tensile surface of a flexure bar in AD-96 alumina. Cavities in this material are not arrested after nucleation, but grow as cracks along grain interfaces. Figure taken from the work presented in reference 16.

Large grains, fibers or whiskers in an otherwise fine grain material promote crack growth over cavity coalescence as a fracture mechanism. The process of crack growth is illustrated in a grade of siliconized silicon carbide (Coors SCRB 210) that contains a mixture of ≈50 μm and ≈3 μm grains of SiC bonded by ≈18 vol. % Si, figure 6 [25]. Generalized cavitation does not occur for this material. Cavities form along the larger grain boundaries and then link up to form a crack. Once the crack has been formed, cavitation occurs preferentially from the crack tip and the material fails by crack growth. Tensile specimens that fail by this process, show no evidence of generalized cavitation within the gauge section. Instead, one or two cracks such as those shown in figure 6 are observed; these usually form at the "higher" stress regions of the gauge section[3].

A similar crack nucleation process is observed in whisker reinforced silicon nitride [27]. In this material, cavities nucleate from the large whiskers and then propagate into the silicon nitride matrix forming a crack that eventually results in component failure, figure 7a. Below a stress threshold, micro cracks, such as that show in figure 7a, do not grow in this material. Cavities are observed at the SiC whisker interface, but these tend to have blunted morphologies, indicating limited growth. Above the crack growth threshold, high densities of

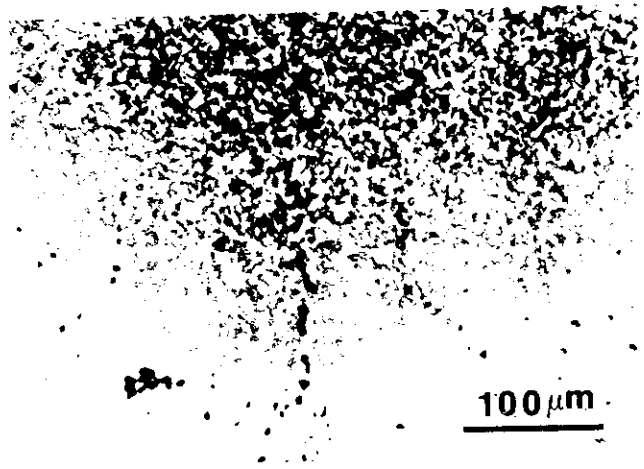

Figure 5. Cavity coalescence in Carborundum KX01. Very few of these coalesced features are observed in the gauge section after testing, suggesting a low probability event. The applied tensile stress is horizontal in this figure.

[3] To reduce stress concentrations in the gauge section, a gradual reduction of the section from the gripping area was used in the design. Never-the-less, an enhancement of stress of approximately 3% is expected [26]. Apparently, this enhancement is sufficient to nucleate cracks at the ends of the gauge section.

microcracks are observed, all of them slowly growing as a function of time, figure 7b. As the applied stress is increased, however, fewer microcracks are observed. Apparently, the crack growth sensitivity of the material to applied stress is greater than the cavity nucleation sensitivity of the material to applied stress, so that a crack, once nucleated, rapidly grows to failure, leaving very little damage behind in the rest of the gauge section.

3. CREEP RUPTURE LIFETIME

Although the lifetime of structural ceramics depends on the exact details of the mechanism responsible for failure, some characteristics of the creep rupture process seem to apply regardless of failure mechanism. Creep rupture studies on a number of structural ceramics indicate, for example, that failure strain is greatest for specimens tested at the slowest strain rates. This relation between failure strain and strain rate is illustrated in figure 8 for three, two phase ceramics. Strains to failure in tension for two phase ceramics tend to be <2%, which means that these materials do not exhibit extended tertiary creep behavior. In fact, primary creep in these materials can be exaggerated, lasting for thousands of hours, when processes such as devitrification occur at grain interfaces [15, 27].

Figure 6. Microcrack formation in Coors SCRB 210. Cavitation appears to occur preferentially at the interfaces of large grains within the structure. This material contains ≈18 vol. % silicon in which are imbedded a mixture of ≈50μm and ≈3μm grains SiC.

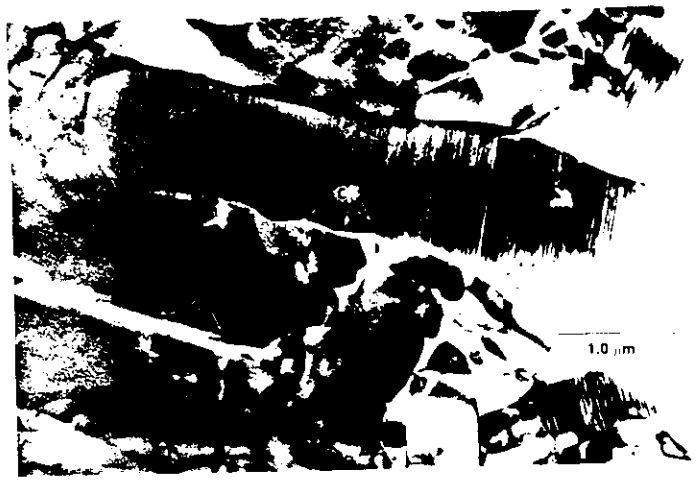

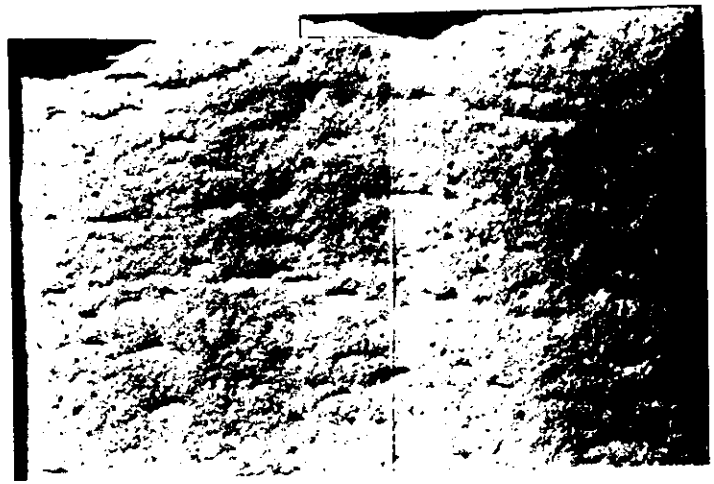

Strain Rate, 1/s

Strain Rate, 1/s

Figure 7. Cavity nucleation in the whisker reinforced materials occurs at the vitreous interfaces bordering the SiC whiskers (a). Cavities grow from the whisker interfaces into the bulk of the material, where they link-up with other cavities eventually forming life-limiting cracks. As can be seen in the polished gauge section of the whisker-reinforced Si_3N_4 specimen in (b), cavities form uniformly throughout the gauge section. The gauge section width is ≈2.5mm. Figure taken from reference 27.

Figure 8.
commer
all three

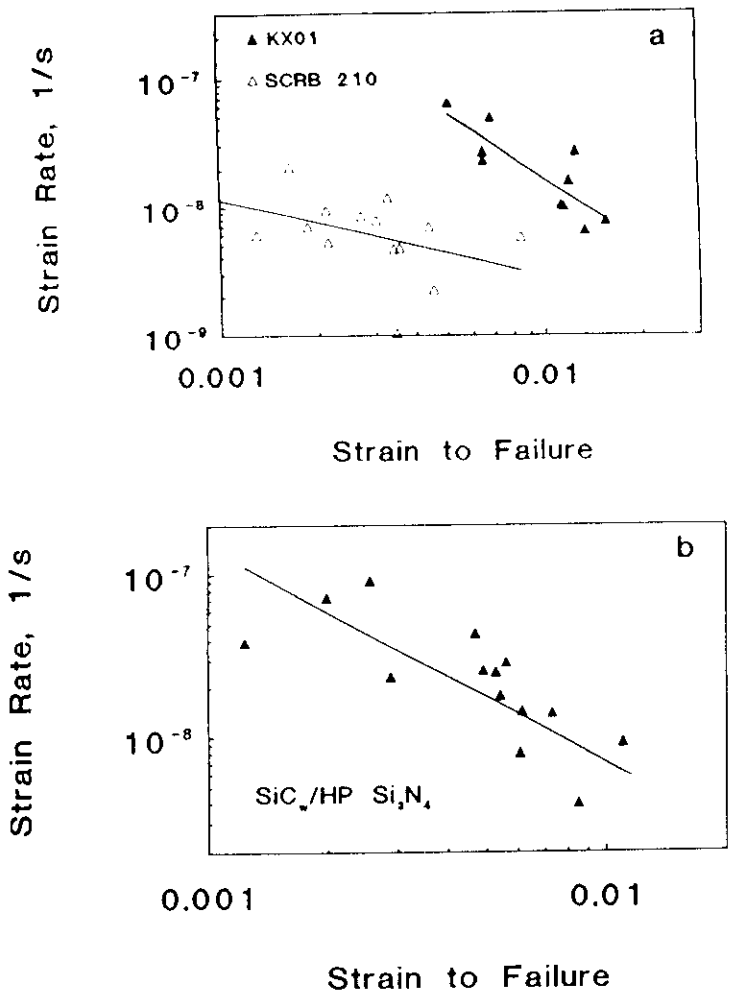

Figure 8. Relation between strain to failure, ε_f, and strain rate, $\dot{\varepsilon}$ (a) two commercial grades of siliconized silicon carbide; (b) SiC_w reinforced Si_3N_4. For all three materials, a greater strain is sustained at lower rates of strain.

With regard to the lifetime of two phase ceramics, a useful observation is that a logarithmic plot of the creep rate versus rupture time often yields a single curve for a material regardless of temperature or applied stress, figure 9. This type of plot was first suggested by Monkman and Grant [14] for the creep rupture of metals. Their data can be represented by a power law relation between rupture time, t_r, and minimum creep rate, $\dot{\varepsilon}$:

$$t_r = C \cdot \dot{\varepsilon}^{-m}, \tag{3}$$

where C and m are empirical constants. The strain rate exponent, m, had a value that ranged from 0.77 to 0.93 for metals studied by Monkman and Grant [14]. The curves for the data presented by Monkman and Grant were independent of stress and temperature, but exhibited a small dependence on the ductility of the metal at fracture. Monkman and Grant noted that most of their data could be represented adequately by setting m = 1, which suggests a constant strain to failure, provided most of the creep strain can be accounted for by strain that develops at the minimum creep rate. A value of 1 for m was observed by Kossowsky et al. [26] in an early study of the tensile creep rupture behavior of hot-pressed silicon nitride. In studies conducted by the present authors, however, values of m were larger than 1. From the data for the three materials plotted in figure 9, values of m were 1.45, 2.39 and 1.69, respectively, for KX01, SCRB210 and SiC_w/Si_3N_4[4]. These values are consistent with the observation that the failure strain decreases with increasing strain rate. Other recent analyses of two phase ceramics show similar Monkman Grant curves for silicon nitride and vitreous bonded aluminum oxide [29]. These results suggest that the Monkman Grant curve is a common feature of creep rupture behavior in two phase ceramics.

The fact that data for ceramic materials fit an equation, such as the Monkman Grant equation, simplifies the analysis of failure mechanisms and the prediction of lifetime. Two equations now describe creep rupture behavior: the creep equation defines the creep process; the Monkman-Grant equation defines the rupture process. Therefore, the mode of deformation and the mode of failure can be analyzed separately. As the Monkman-Grant equation is independent of stress and temperature, the temperature and stress dependence of the creep rupture behavior will depend only on the creep behavior of the ceramic. Furthermore, if the Monkman-Grant curve is also a universal relation for a given type of material, then improvements in lifetime can be achieved solely by improving the creep resistance of the solid.

The Monkman-Grant equation and the creep equation can be combined to provide an estimate of the failure time as a function of applied stress and temperature. Thus, if $t_r = C \cdot \dot{\varepsilon}^{-m}$, and $\dot{\varepsilon} = \dot{\varepsilon}_o \cdot e^{-Q/RT} \cdot (\sigma/\sigma_o)^n$, then $t_r = C \cdot \dot{\varepsilon}_o^{-m} \cdot e^{mQ/RT} \cdot (\sigma/\sigma_o)^{-mn}$, so that both the apparent activation energy and the stress exponent for the failure time can be calculated from those for the creep rate. Obtaining the Monkman-Grant data and the creep data separately permit the failure time to be obtained as a function of stress more efficiently than if

[4] The identification of commercial grades of ceramics is not to be construed as endorsement by the National Institute of Standards and Technology.

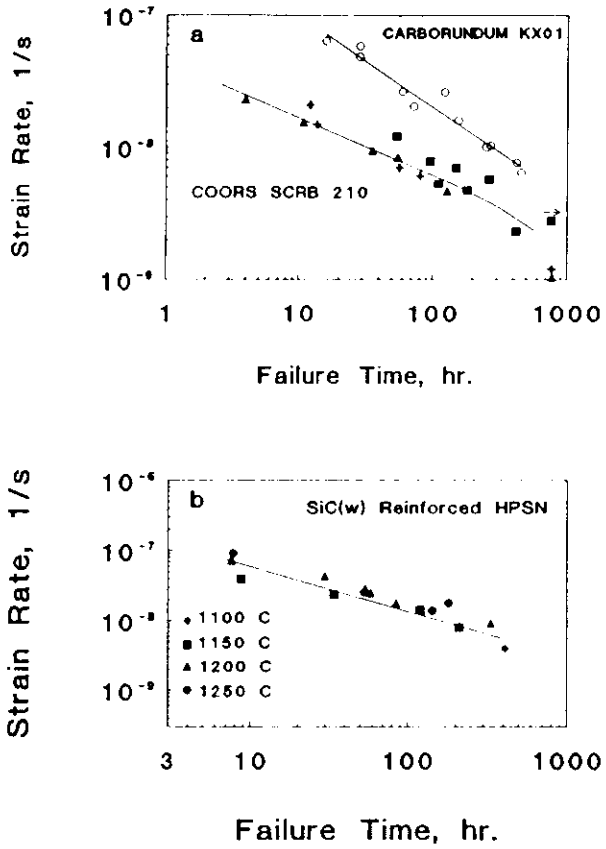

Figure 9. Creep rupture behavior of (a) siliconized silicon carbide and (b) SiC_w reinforced Si_3N_4. The three sets of data were taken over a range of stresses and temperatures. Regardless of the test conditions, data for each material cluster about a single curve. The strain exponents for the two grades of Si/SiC are 1.45 for the Carborundum KX01 and 2.39 for the Coors SCRB 210 (data from reference 25). The arrow over the data point in the lower right hand part of figure 9a indicates a specimen that was discontinued after ≈800 hr. The strain exponent for the SiC_w/Si_3N_4 is 1.69 (data from reference 27).

they were collected directly. This conclusion follows from the fact that only a small number (e.g. 6) of creep-rupture tests are required to define the Monkman-Grant curve. If multiple creep experiments can be used on individual specimens, an even smaller set of specimens (e.g. 2) can be used to define the stress and temperature dependence of the creep rate. Thus, a relatively rapid initial assessment of the creep behavior of a solid can be obtained from a limited number of samples.

4. MECHANISMS OF FAILURE IN TWO PHASE CERAMICS

Data presented in this paper suggest that the failure of two phase ceramics can be characterized by two extremes in behavior. In materials that contain a large volume fraction of bonding phase, cavities tend to nucleate at grain interfaces and then stabilize after growing into full facet cavities. Failure in this mode is by cavity coalescence to form a critical size crack. Once a critical crack is formed, crack growth is relatively rapid, so that failure is determined by the time required for the cavities to coalesce into cracks.

At the other extreme, failure is caused by creep crack nucleation and propagation. In these microstructures, interfacial cavitation followed by rapid interfacial cavity growth to form crack nuclei is favored. This occurs for materials that have relatively small amounts of second phase, or in materials that contain whiskers or large grains. The rate limiting step for component lifetime can be crack nucleation, or crack growth, or a combination of the two. As an example, in vitreous bonded alumina containing 8 vol. % vitreous phase (Coors AD96), ≈33% of the failure time is required for cavity nucleation, indicating that both processes determine the lifetime [30]. Similar studies have yet to be conducted on other materials.

4.1. Failure by crack Growth

A relatively simple derivation of a Monkman-Grant equation can be obtained if the time for nucleating cracks is assumed to be short relative to the time for crack growth[5]. As an extreme of this condition, we consider creep failure from pre existing flaws. If the crack growth rate is a power function of the applied stress intensity factor, i.e. $v = v_o \cdot \exp(-Q/RT) \cdot (K_I/K_o)^n$, then the time to failure, t_f, is given by $t_f = B \cdot \exp(Q/RT) \cdot S_i^{n-2} \cdot \sigma^{-n}$, where B is a materials/environmental constant and S_i is the strength determined from the initial flaw size [4]. Combining this equation with the Norton equation for creep, $\dot{\varepsilon} = \dot{\varepsilon}_o \cdot e^{-Q/RT} \cdot (\sigma/\sigma_o)^n$, the following equation is obtained for the time to failure[6]:

$$t_f = \varepsilon^{1/n} \cdot B \cdot e^{[(n/n)(n-Q)/RT]} \cdot S_i^{n-2} \cdot [\sigma_o^n/\dot{\varepsilon}_o]^{1/n} \qquad (4)$$

[5] For crack growth to be an important mechanism of failure, either crack growth must initiate from pre-existing defects, in which case the nucleation time is zero, or a fixed but small number of nucleation sites must be present. Once these sites are activated, the remaining lifetime is determined by crack growth from these sites.

[6] This approach to component lifetime was first suggested by Lange [32].

From this equation, the strain rate exponent for the Monkman-Grant equation is m = p/n. Furthermore, the coefficient C in the Monkman-Grant equation (equation 3) is temperature independent only if H/n = Q/p. Otherwise, a series of parallel lines will be obtained on a Monkman-Grant type of plot.

Equation 4 provides a means of estimating the Monkman-Grant exponent directly from creep and crack growth measurements. The exponent for the creep rate, n, can be obtained from tensile creep measurements. The crack growth exponent can be obtained from indentation cracks in tensile bars, or from fracture mechanics specimens. However, as indentation cracks may not propagate in the same way as those that nucleate naturally during creep, it is probably better to obtain the crack growth exponent from naturally nucleated cracks. The fact that these two types of cracks may behave differently during creep was demonstrated on flexural bars of vitreous bonded alumina (Coors AD96) by Jakus et al. [30]. As shown in figure 10, the stress intensity factor exponent of the crack propagation rate was 4 for artificially introduced indentation cracks, but only 1 for natural cracks generated by the creep process[7]. Recently, Jakus and Nair [31] demonstrated the same type of behavior on SiC whisker reinforced Al_2O_3. Results shown in figure 10 should be confirmed on tensile specimens because of the greater simplicity of the stress distribution in this type of loading. Despite this precaution, equation 4 provides a useful representation for creep rupture under conditions when lifetime is determined primarily by crack propagation parameters.

4.2. Failure by Cavity Coalescence

The following sequence of events is consistent with observations of cavitation damage in Carborundum KX01 [17, 18]. Prior to coalescence, cavities form at random throughout the gauge section. At small strains, cavities are isolated, but stable. With increasing strain, the cavity density increases and some cavities are nucleated adjacent to others, thus, forming small cracks. When a sufficient number of cavities are linked together, a self sustaining crack is formed which then propagates to failure. At any time, the size of the crack that forms depends on the density of the cavities and therefore on the creep strain. If a relationship between creep strain and critical crack size can be developed, then, as shown below, the time to failure can be determined solely from the creep behavior of the material.

An estimate of the crack size can be obtained from total creep strain by a two step process. First, the cavity density is determined experimentally as a

[7] This kind of behavior cannot be rationalized on the basis of stress relaxation in the surface of the flexure beam. Stresses in the beams that contain the indentation cracks are expected to be higher during crack growth, since the indentation cracks are present for the entire period of testing, whereas the naturally grown cracks form after the stress field in the flexure bar has relaxed. With the higher stress, a higher crack velocity would be expected for a given applied stress intensity factor, in contrast to what is observed in figure 10.

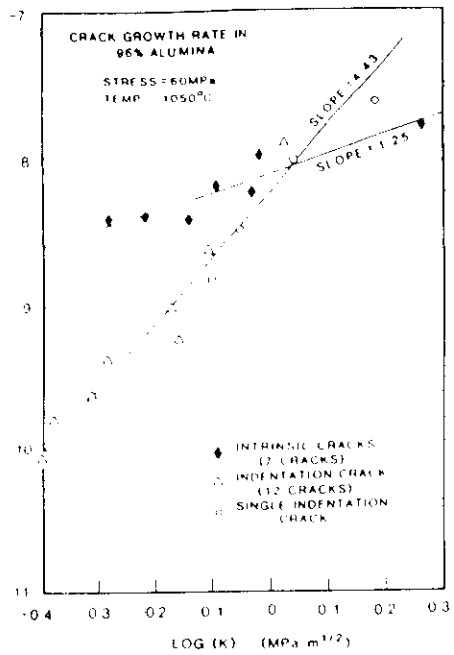

Figure 10. Crack propagation curves for both creep nucleated and indentation nucleated cracks in vitreous bonded aluminum oxide (AD 96). The slope of the curve for the indentation-nucleated cracks is about 4 times that of the curve for creep-nucleated cracks. Data taken from reference 30.

function of total strain, either by density measurements or by ceramographic techniques. Then, the crack size is estimated from the cavity density by using statistical theory. Recently, Carroll and Tressler [18] determined the cavity density in siliconized silicon carbide specimens (Carborundum KX01) that were strained in tensile experiments conducted at 1100°C (versus 1225°C to 1400°C for the creep rupture data shown in figure 9). The cavity density was found to be linearly related to the total strain in the gauge section of the specimen, figure 11. A positive intercept on the strain axis of the data suggests a finite strain for cavitation. A linear relation between cavity density and creep strain has also been reported in other studies on ceramic materials [33 ,34]. Using the cavity density data in figure 11 and the strain to failure date in figure 8, it can be concluded that the density of cavities at failure ranged from ≈680/mm^2 (ε=0.004) to ≈3000/mm^2 (ε=0.014).

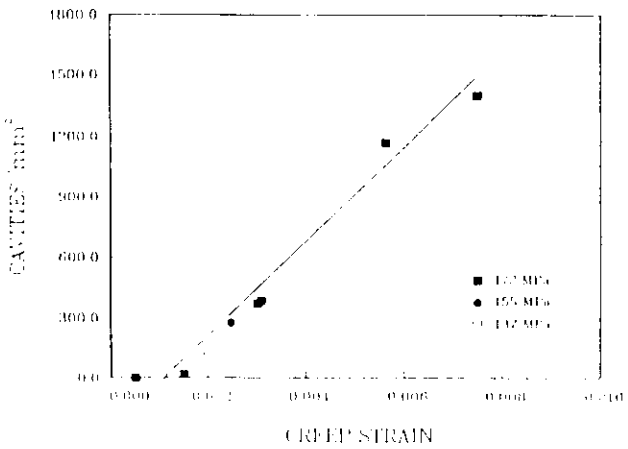

Figure 11. Area density of cavities as a function of creep strain at 1100°C. The fraction of cavitated grains, p, was estimated as the density of cavities divided by density of grains per unit area of surface.

The relation between cavity density and crack size can be determined from the statistical analysis of Lindborg[8] [35]:

$$f = 0.2(2 \cdot q/N)^{1/q}, \qquad (5)$$

where f is the fraction of grains cavitated in the solid and N is the total number of grain boundaries normal to the applied stress. q is the cluster size, i.e. the number of cavities aggregated together to form a crack. If the gain size, G, is assumed to be uniform throughout the solid, and if the grains are arranged in a cubic lattice, then $N = (W/G)^2 \cdot (L/G)$, where W is the width of the gauge section, which is assumed to be square, and L is the length of the gauge section . The area occupied by a cluster is just $G^2 \cdot q$, and the crack size, 2a, is assumed proportional the square root of the cluster area, $G \cdot \sqrt{q}$.

[8] See the paper by Hunt [36] for a critical discussion of Lindborg's work. In deriving equation 5 the implicit assumption is made that failure occurs once a critical failure probably is reached, ≈60-70%. This same assumption was used in a paper by Rana and Evans [13] in their discussion of failure by cavity coalescence.

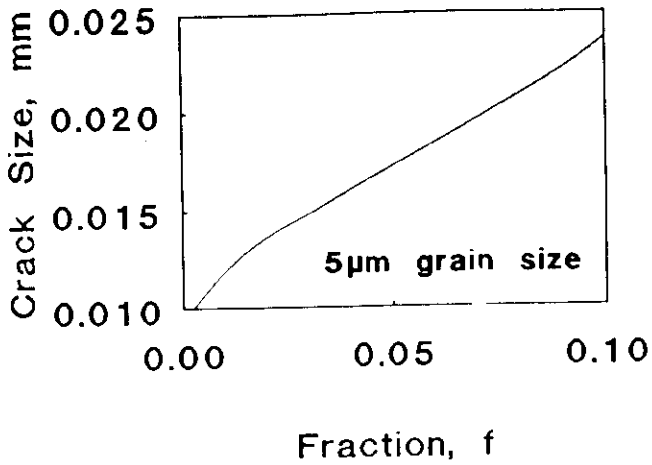

Figure 12. Calculated crack size as a function of the fraction of cavitated grains. This curve is a plot of equation 5, for which the crack size, 2a, is equal to $G \cdot \sqrt{q}$, the grain size, G, is equal to 5μm and the total number of boundaries, N, normal to the applied stress is equal to $1x10^4$ (assuming W 3mm and L 15mm).

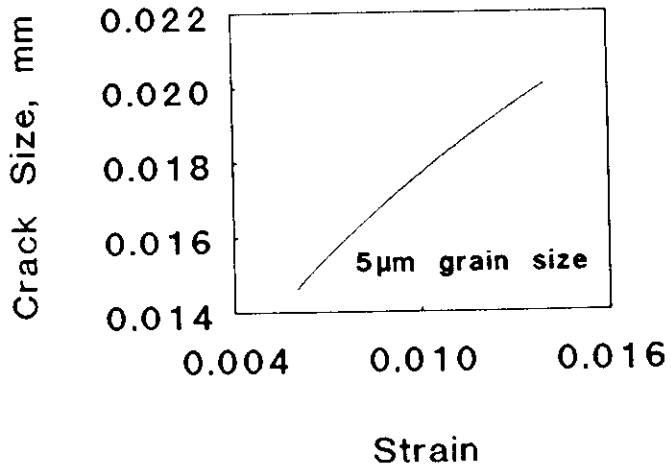

Figure 13. Calculated crack size as a function of specimen strain. This figure is obtained by using the curves in figures 11 and 12 to eliminate the fraction of cavitated grains as a variable.

Using the above definitions, equation 5 is plotted in figure 12, where the crack size, 2a, is the ordinate and the fraction of cavitated boundaries, f, is the abscissa. This equation is nonlinear; the crack size, 2a, approaches infinity as f approaches 0.2. Therefore, f=0.2 is an upper bound for the fraction of ruptured boundaries in a solid. In the set of experiments on Carborundum KX01, the cluster size was much smaller than this value. The range of values estimated above for the cavity density at failure is ≈680/mm^2 to ≈3000/mm^2. Assuming the grains may be represented by stacked cubes 5μm on a side, the grain boundary density is 40x10^3/mm^2. Combining these two estimates, the fraction of cavitated boundaries at fracture ranged from ≈0.017 to ≈0.076. For this range of f, the critical crack size ranges from ≈13 to ≈20μm, suggesting a cluster size of from ≈7 to ≈16 for a self sustaining crack.

Combining the data in figure 11 with the theoretical curve in figure 12, an estimate of the dependence of crack size on strain is obtained, figure 13. A power law fit to the points in figure 13 yields the following equation for the estimated crack size as a function of strain:

$$2a = b \cdot \varepsilon^{-m} \qquad (6)$$

where b has the value 1x10^{-3}μm.

Equation 6 may now be combined with empirical representations of the creep data to obtain an equation for the creep rupture behavior. The creep data shown in figure 14 for Carborundum KX01 is linearized, $\varepsilon_{cr} = \dot{\varepsilon} \cdot t_r$, since the linear equation represents the creep data over approximately 80 percent of the

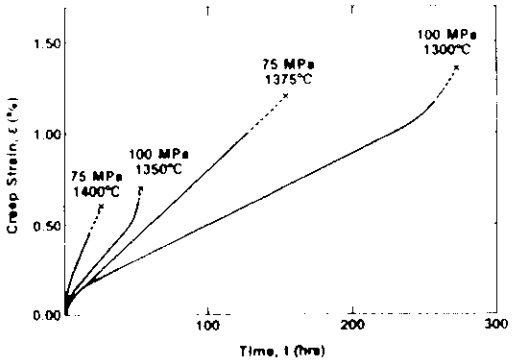

Figure 14. Uniaxial creep curves for KX01 at various thermal and mechanical loadings. Three important observations can be made from this data: (1) over most of the data range, creep strain can be represented as a linear function of time; (2) rupture strain decreases with increasing creep rate; (3) the maximum rupture strain is ≈1.5%, which indicates brittle behavior even at low rates of creep. Figure from reference 38.

lifetime of each specimen. The stress dependence of the creep behavior is represented by the Norton equation: $\dot{\varepsilon} = \dot{\varepsilon}_o \cdot (\sigma/\sigma_o)^n$, where $\dot{\varepsilon}_o$ now contains the temperature dependence of the creep rate. For experiments on KX01, n = 11. If σ_o is selected as 100 MPa, then $\dot{\varepsilon}_o = 1x10^{-8}s^{-1}$.

Finally, at some threshold stress intensity factor, K_{th}, a crack is assumed to grow from a coalesced nucleus. The crack nucleus is defined by: $K_{th} = (2/\sqrt{\pi}) \cdot \sigma \cdot \sqrt{a}$, where a is the critical crack radius. Combining these equations, the relationship between creep rate and rupture time is given by the following equation:

$$\varepsilon^{(n/n+1)} \cdot t_r = [(n/2b)^{1/2} \cdot (K_{th}/\sigma_o) \cdot \dot{\varepsilon}_o^{1/n})]^{n/n+1} \qquad (7)$$

The form of this equation is identical to that of a Monkman Grant equation, with m = 1+5.3/n. Since n ≈ 11 in the present experiment [18], m ≈ 1.48, which compares favorably with the value of 1.45 obtained from the creep rupture data shown in figure 9.

Once the value of m is determined, the right hand side of equation 7 can be evaluated and K_{th} can be determined. In the current experiment, $K_{th} \approx 0.4$ MPa m$^{1/2}$, which is consistent with a value of 2a ≈ 22 μm for the critical crack size. This value of K_{th} is much lower than the value of K_{Ic} measured on chevron notched specimens of this material tested at elevated temperatures. At 1300°C, for example, K_{Ic} for KX01 is ≈15 MPa m$^{1/2}$ [37]. This value of K_{Ic} is a consequence of a substantial cavitation zone that develops around the crack tip in these materials at elevated temperatures. These zones are readily observed in siliconized silicon carbide at the tips of cracks at freshly introduced indentations, figure 15. For these cracks, propagation is preceded by the

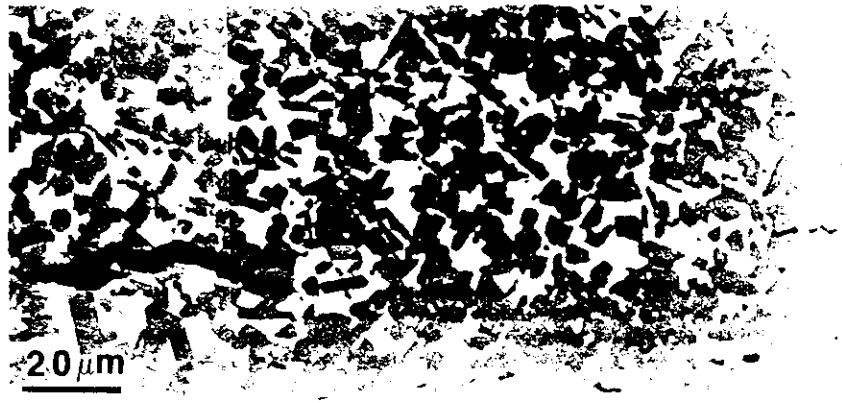

Figure 15. Cavity distribution around the tip of an indentation crack in KX01. Cavities form a cloud around the crack tip, which later link up as the crack propagates (Vickers indentation, 10 kg; temperature 1300 C; stress 120 MPa; time under load 19 hr).

linkage of cavities with the crack tip. Thus, plastic work at the crack tip, and volume expansion accompanying cavitation probably account for the high toughness of this material at elevated temperature. By contrast, cracks that nucleate within the creeping material as a consequence of creep , do not develop large cavitated zones as they propagate, figure 5, which again suggests a basic difference in behavior between cracks freshly introduced into an unstrained material, and cracks that develop as a consequence of the creep behavior of the materials. Creep apparently "work hardens" ceramic materials, embrittling them and reducing resistance to crack growth. As in the case of the alumina tested in flexure [30], self nucleated cracks appear to propagate differently from ones that are introduced by indentation.

5. SUMMARY

Two types of creep-rupture behavior are observed in two phase structural ceramics. Ceramics that contain large amounts of bonding phase form distributed isolated cavities during creep. With continuing creep, the density of cavities increases. Cavities link to form critical size cracks that eventually cause failure. As the amount of bonding phase is decreased, constraints are such that cavities, once nucleated, propagate as cracks. Small amounts of bonding phase in the material effectively embrittle ceramics at elevated temperatures reducing strain to failure. The strain to failure is also reduced if large grains or fibers are included within the solid, as these are preferred sites of cavity nucleation and rapid growth into cracks. Regardless of fracture mechanism, however, lifetime can be expressed as a power function of the creep rate, independent of temperature or applied stress. This separation of creep rupture behavior into creep behavior and rupture behavior simplifies the analysis of creep rupture data and permits a more rapid evaluation of material performance for high temperature application.

Acknowledgement: Support of the Ceramic Technology for Advanced Heat Engines Program, U.S. Department of Energy, and Test Methodology for Tubular Components Program of the Gas Research Institute is gratefully acknowledged.

REFERENCES

[1] A.G. Evans (1985) "Engineering Property Requirements for High Performance Ceramics," Mat. Sci. and Eng. **71** 3-21.

[2] A.G. Evans and B.J. Dagleish, "Some Aspects of the High Temperature Performance of Ceramics and Ceramic Composites," pp. 929-955 in **Creep and Fracture of Engineering Materials and Structures**, B. Wilshire and R.W. Evans Eds. The Institute of Metals, London (1987).

[3] G. Grathwohl, "Creep and Fracture of Hot-Pressed Silicon Nitride with Natural and Artificial Flaws," pp. 565-577 in **Creep and Fracture of Engineering Materials and Structures**, Edited by B. Wilshire and R. Owen, Pineridge, Swansea, U.K. (1984).

[4] S.M. Wiederhorn and E.R. Fuller, "Structural Reliability of Ceramic Materials," Mater. Sci. and Eng. **71** 169-186 (1985).

[5] G. Quinn (1984) "Static Fatigue in High-Performance Ceramics," pp.177-193 in **Methods for Assessing the Structural Reliability of Brittle Materials**, ASTM STP 844, S.W. Freiman and C.M. Hudson, Eds.

[6] M.D Thouless and A.G. Evans (1986) "On Creep Rupture in Materials Containing an Amorphous Phase," Acta Metall. **34** 23-31.

[7] M.D. Thouless (1987) "A Review of Creep Rupture in Materials Containing an Amorphous Phase," Res Mechanica **22** 213-242.

[8] T.L. Tsai and R. Raj (1982) "Creep Fracture in Ceramics Containing Small Amounts of a Liquid Phase," Acta Metall. **30** 1043-1058.

[9] R. Raj and M.F. Ashby (1975) "Intergranular Fracture at Elevated Temperature," Acta Metall. **23** 653-666.

[10] J.R. Porter, W. Blumenthal and A.G. Evans (1981) "Creep Fracture in Ceramic Polycrystals - I. Creep Cavitation Effects in Polycrystalline Alumina," Acta Metall. **29** 1899-1906.

[11] C.H. Hsueh and A.G. Evans (1981) "Creep Fracture in Ceramic Polycrystals - II. Effects of Inhomogeneity on Creep Rupture," Acta Metall. **29** 1907 1917.

[12] M. Thouless and A.G. Evans (1984) "Nucleation of Cavities during Creep of Liquid-Phase-Sintered Materials," J. Am. Ceram. Soc. **67** 721-727.

[13] A.G. Evans and A. Rana (1980) "High Temperature Failure Mechanisms in Ceramics," Acta Metall. **28** 129-141.

[14] F.C. Monkman and N.J. Grant (1956) "An Empirical Relationship between Rupture Life and Minimum Creep Rate in Creep-Rupture Tests," Proc. ASTM **56** 593-620.

[15] D.S. Cranmer, B.J. Hockey, and S.M. Wiederhorn, "Creep and Creep-Rupture of Hot Isostatically Pressed Silicon Nitride," to be published.

[16] S.M. Wiederhorn, B.J. Hockey and R.F. Krause, Jr., (1987) "Influence of Microstructure on Creep Rupture"; pp. 795-806 in **Ceramic Microstructures '86: Role of Interfaces**, edited by J.A. Pask and A.G. Evans, Plenum Press, New York.

[17] S.M. Wiederhorn, D.E. Roberts, T.-J. Chuang, and L. Chuck (1988) "Damage Enhanced Creep in Siliconized Silicon Carbide: Phenomenology," J. Am. Ceram. Soc., **71** 602-608.

[18] D.F. Carroll, and R.E. Tressler (1988) "Accumulation of Creep Damage in a Siliconized Silicon Carbide," J. Am. Ceram. Soc. **71** 472-477.

[19] D.C. Drucker (1965) "Engineering and Continuum Aspects of High-Strength Materials"; pp. 795-833 in **High Strength Materials**, edited by V.F. Zackay, Wiley, New York.

[20] F.F. Lange (1972) "Non-Elastic Deformation of Polycrystals with a Liquid Boundary Phase"; pp. 361-81 in **Deformation of Ceramic Materials**, edited by R.C. Bradt and R.E. Tressler, Plenum Press, New York.

[21] A.H. Cottrell (1964) **The Mechanical Properties of Matter**, John Wiley and Sons, New York.

[22] H.J. Frost and M.F. Ashby (1982) **Deformation-Mechanism Maps: The Plasticity and Creep of Metals and Ceramics**, Pergamon Press, Oxford.

[23] B.J. Dalgleish, S.M. Johnson and A.G. Evans (1984) "High-Temperature Failure of Polycrystalline Alumina: I, Crack Nucleation," J. Am. Ceram. Soc. **67** 741-750.

[24] D.S. Wilkinson, A.G. Robertson and C.H. Cáceres, "Damage Mechanisms during High Temperature Creep in Hot-Pressed Alumina," to be published.

[25] S.M. Wiederhorn, W. Liu, D.F. Carroll, D.F., and T.-J. Chuang (1989) "Creep Rupture of Two Phase Ceramics," Presented at the 91st Annual Meeting and Exposition of the American Ceramic Society, April 23- 27, Paper 7-JIII-89.

[26] R.E. Peterson (1974) **Stress Concentration Factors**, Wiley-Interscience, New York.

[27] B.J. Hockey S.M. Wiederhorn, W. Liu, J.G. Baldoni and S.-T. Buljan, "Tensile Creep of Whisker-Reinforced Silicon Nitride," J. Mat. Sci., in press.

[28] R. Kossowsky, D.G. Miller, and E.S. Diaz (1975) "Tensile and Creep Strengths of Hot-Pressed Si_3N_4," J. Mat. Sci. **10** 983-997.

[29] M.K. Ferber, M.G. Jenkins and V.J. Tennery (1990) "Comparison of Tension, Compression, and Flexure Creep for Alumina and Silicon Nitride Ceramics," Ceram. Eng. Sci. Proc. **11** 1028-45.

[30] K. Jakus, S.M. Wiederhorn and B.J. Hockey (1986) "Nucleation and Growth of Cracks in Vitreous Bonded Aluminum Oxide at Elevated Temperatures," J. Am. Ceram. Soc. **69** 725-31.

[31] K. Jakus and S.V. Nair (1990) "Nucleation and Growth of Cracks in SiC/Al_2O_3 Composites," Comp. Sci. and Technol. **37** 279-97

[32] F.F. Lange (1976) "Interrelations between Creep and Slow Crack Growth for Tensile Loading Conditions," Int. J. Fracture **12** 739-744.

[33] E. Messner (1990) "Kriechverhalten und Kreichporenbildung von heissgepresstem Siliciumnitrid," Ph.D. Thesis, Technischen Universität Hamburg-Harburg.

[34] J. Stark (1988) "Verfomungsverhalten und Kriechporenbildung von reinem und glasphasehaltigem Aluminiumoxid," Ph.D. Thesis, Technischen Universität Hamburg-Harburg.

[35] U. Lindborg (1969) "A Statistical Model for the Linking of Microcracks," Acta Metall. **17** 521-526.

[36] R.A. Hunt (1978) "A Theory of the Statistical Linking of Microcracks Consistent with Classical Reliability Theory," Acta Metall. **26** 1443-1452.

[37] K. Kromp, T. Haug, R.F. Pabst and V. Gerold (1987) "C^* for Ceramic Materials? Creep Crack Growth at Extremely Low Loading Rates at high Temperatures using Two-Phase Ceramic Materials," pp. 1021-1033 in **Creep and Fracture of Engineering Materials and Structures**, B. Wilshire and R.W. Evans, Eds., The Institute of Metals, London.

[38] T.-J. Chuang, D.F. Carroll and S.M. Wiederhorn (1989) "Creep Rupture of a Metal-Ceramic Particulate Composite," pp. 2965-2976 in **Advances in Fracture Research**, Proceedings of the 7th International Conference on Fracture (ICF7), K. Salama, K. Ravi-Chandar, D.M.T. Taplin, P. Rama Rao, Eds., Houston, Texas, 20-24 March 1989, Pergamon Press, New York.